Oxford OUTP-93-22P
CERN-TH-6995/93
TUM-TH-159/93

LARGE SCALE STRUCTURE FROM BIASED NON-EQUILIBRIUM PHASE TRANSITIONS – PERCOLATION THEORY PICTURE

Z. Lalak[a,b], S. Lola[a], B. A. Ovrut[c] and G. G. Ross[a,1]

[a] Dept. of Physics
Theoretical Physics
University of Oxford
1 Keble Road, Oxford, OX1 3NP

[b] Physics Department
Technische Universität München
D-85748 Garching

[c] Theory Division CERN
CH-1211 Geneva 23

ABSTRACT

We give an analytical description of the spatial distribution of domain walls produced during a biased nonequilibrium phase transition in the vacuum state of a light scalar field. We discuss in detail the spectrum of the associated cosmological energy density perturbations. It is shown that the contribution coming from domain walls can enhance the standard cold dark matter spectrum in such a way as to account for the whole range of IRAS data and for the COBE measurement of the microwave background anisotropy. We also demonstrate that in case of a biased phase transition which allows a percolative description, the number of large size domain walls is strongly suppressed. This offers a way of avoiding excessive microwave background distorsions due to the gravitational field of domain walls present after decoupling.

[1] SERC Senior Fellow

1. Introduction

Over the years there has been considerable effort put into explaining the observed large scale structure of the Universe. Recently, interest in the subject has been greatly stimulated by new data coming from the positive signal from COBE [1] and from the extensive IRAS survey [2]. Perhaps one of the most interesting new conclusions is the lesson that the standard cold dark matter (CDM) scenario with a Harrison-Zeldovich spectrum of primeval fluctuations apparently cannot alone account for the whole spectrum of observed energy density fluctuations [3],[4]. If one normalizes the CDM spectra so as to explain the data on very small scales, then there are not sufficient fluctuations predicted at larger scales to be consistent with the large scale IRAS results, let alone to offer any possible explanation of the COBE measurements. The discrepancy is significant, despite the fact that data on larger scales also have large errors, of the order of 20% of the critical density at 40–50 Mpc and about 10% of the critical density at 100 Mpc (assuming $H_0 = 100$ kmsec^{-1}Mpc^{-1}). On the particle theory side, there have been several attempts to supply more power to the long wavelength parts of the theoretical spectrum [3],[5]. Some of them replace pure CDM with a mixture of CDM, hot and warm dark matter while others use topological defects created during cosmological phase transitions to depart from CDM-like predictions. In this work, we perform a detailed analysis of density perturbations produced by biased, non-equilibrium phase transitions in the vacuum state of a light weakly interacting scalar field. We consider domain walls formed during such a transition, and argue that under quite general circumstances they act as bag-like seeds for density inhomogeneities of the baryonic and cold dark matter filling the Universe. Our statistical method, based on percolation theory, allows us to formulate a quantitative picture for structure formation, and to perform an analytical calculation of the theoretical spectrum. In a natural way, we obtain predictions for the overdensity arising from these domain walls. When this is added to the CDM spectrum, we obtain a remarkably accurate prediction for the total density fluctuations which is consistent with the entire range of the IRAS data and, simultaneously, with the COBE measurements. We stress that these results are obtained using domain walls which are perhaps the most natural kind of topological defects, easily accomodated by a large class of realistic models [6].

The scalar field we introduce is assumed to interact only gravitationally with the rest of matter, and to have very weak self interactions. Hence this field is never in thermodynamic equilibrium. For this reason our theory escapes all previous no-go results for cosmological domain walls. We will, henceforth, refer to such a scalar field as a "structuron", since its main physical role is the creation of large scale structure. Furthermore, although the associated phase transition encompasses the so-called late-time phase transitions, it is actually much more general. In particular, our transition can occur at any time, such as well before photon decoupling, in distinction to late-time transitions which only occur long after recombination. A further difference is that the non-equilibrium nature of our transition allows us to bias the preference of the theory to choose one vacuum state over another. In the original late-time transitions the vacuum states were populated with equal probabilities. For these reasons, we will refer to the out of equilibrium phase transitions of the structuron as "structure transitions". In this paper the structure transition will in fact occur prior to photon decoupling.

The paper is organized as follows. In sections 2 and 3 we recapitulate basic facts about domain walls and elements of percolation theory relevant in cosmology. In section 4 we sketch the generic inflationary mechanism for producing domain wall patterns leading to realistic energy density spectra. In section 5 we calculate analytically these spectra while in section 6 we perform fits to observational data in the context of realistic particle physics models. In section 7 we comment on the possible sources of microwave background distortions which arise in our scenario. Finally, section 8 contains a brief summary and presents our conclusions.

2. Domain Walls

Domain walls, which are planar defects in the vacuum alignment over space, can appear if the manifold $\mathcal{M}$ of degenerate (or nearly degenerate) vacua of the theory is disconnected, that is, when $\pi_0(\mathcal{M})$ is nontrivial. This is in general the case if there is a discrete symmetry in the theory. This symmetry can be fundamental as, for example, is the $\phi \rightarrow -\phi$ discrete symmetry in the double-

well potential

$$V(\phi) = \frac{\lambda}{4}\upsilon^4(\frac{\phi^2}{\upsilon^2} - 1)^2 \tag{1}$$

It may also arise dynamically during the breakdown induced by instanton effects of a continuous symmetry, such as $\phi \rightarrow \phi + c$, for example by QCD-like gauge instantons or Dirac-type monopoles in antisymmetric tensors. Moreover, discrete symmetries are often left over after an explicit breaking of a continuous symmetry due to Yukawa-type interactions as in the case of classical pseudogoldstone bosons or due to higher-order nonrenormalizable interactions which often happens in string-inspired models[5]. In all these cases the resulting multi-well potential is of the form

$$V = V_0[\cos\left(\frac{\phi}{\upsilon}\right) + 1] \tag{2}$$

which breaks the continuous symmetry down to the discrete symmetry $\phi \rightarrow \phi + 2\pi m\upsilon,\ m = 1, 2, \ldots$. The potential (2) has a finite number of distinct degenerate minima if ϕ is an angular-type degree of freedom or an infinite number of inequivalent minima if the manifold spanned by ϕ is noncompact. The results of this paper are generic to all theories of the above types. In fact, it is not even necessary that the nonequivalent minima be exactly degenerate, so the symmetries we consider may be only approximate ones, although non-degeneracy may change the details of the wall evolution[5]. However, as we have noted, many reasonable models give rise naturally to cosine potentials. Therefore we will use potential (2) in the explicit calculations in this paper. As will become clear below, even though such potentials can have a large number of inequivalent degenerate minima, in this paper we need only consider two adjacent vacua.

The equation of motion corresponding to (2) admits kink- like, static domain wall solutions that interpolate between two adjacent vacua. Locally, we can consider these walls as lying in the $x - y$ plane. In this case the static domain wall solution between the two vacua $\phi_{+,-} = +\pi\upsilon,\ -\pi\upsilon$ is given by

$$\phi_{wall}(z; z_0) = 2\upsilon\ \arctan(\sinh(\frac{z - z_0}{\Delta})) \tag{3}$$

where z_0 is the arbitrary location of the wall, Δ is its width,

$$\Delta = \frac{\upsilon}{\sqrt{V_0}} = m^{-1} \tag{4}$$

and m is the mass of ϕ evaluated at any minimum. The surface energy density of the wall is easily computed to be

$$\sigma = \int_{-\infty}^{+\infty} V_0 \left[\cos\left(\frac{\phi_{wall}}{\upsilon} \right) + 1 \right] dz = 8\,\upsilon^2 m \tag{5}$$

Of course, an arbitrary spatial superposition of domain walls, such as that produced by the physical mechanism described in this paper, is not a solution to the equation of motion and cannot be stable. However, we argue that such a superposition represents physically meaningful initial conditions, whose subsequent evolution is governed by the dynamics of the theory. Subject to this dynamics, the initially static domain walls acquire non-zero velocities and oscillate under their surface tension. The basic features of domain wall evolution relevant for our calculations are discussed and applied in sections 5 and 6.

3. Basics of Percolation Theory

Consider three-dimensional space partitioned into cubic lattice sites with lattice spacing Λ. We will assume that at each lattice site the physical system can be in one of two vacua, which we will call $(+)$ and $(-)$ respectively. The probability that a lattice site is in the $(+)$ vacuum is denoted by p where $0 \leq p \leq 1$, while the probability that a lattice site is in the $(-)$ vacuum is $q = 1 - p$. If there is no correlation between the vacuum structures at any two different lattice sites, it is possible to calculate the spatial distribution of the two vacua, and, hence, the spatial distribution of domain walls by applying three-dimensional percolation theory.

In [7] it has been shown that as long as $p < p_c$, where $p_c = .311$ is the critical probability for a cubic lattice in three dimensions, the $(-)$ vacua lie predominantly in a large percolating cluster (since necessarily $q > p_c$) while the $(+)$ vacua are in finite s-clusters. Here s denotes the number of nearest neighbour lattice sites that are occupied by $(+)$. Two sites are considered nearest neighbours if they have a common link. Also, as $p \to p_c$ from below, large pre-incipient percolating clusters of $(+)$ vacua may begin to form in a finite lattice. However, this happens only for p very close to p_c. Since, in our discussion, we always take p much smaller than p_c, we need not discuss this subtlety further.

Let $n_s(p)$ be the probability per lattice site that a given lattice site is an

element of an s-cluster. This is a fundamental quantity, given by the ratio of the total number of s-clusters, N_s, over the total number of lattice sites, N. An analytical expression for this quantity has been found, [7], using scaling arguments and Monte Carlo simulations. The result is

$$n_s(p) = .0501 s^{-\tau}\ e^{-.6299(\frac{p-p_c}{p_c})s^{\sigma}[(\frac{p-p_c}{p})s^{\sigma}+1.6679]} \tag{6}$$

where $\tau = 2.17$ and $\sigma = .48$. The average radius of gyration for an s-cluster $R_s(p)$, for $p < p_c$ and $s > s_\xi$, is found to be

$$R_s(p) \equiv f_s(p)\Lambda = .702(p_c - p)^{.322} s^{.55}\Lambda \tag{7}$$

where

$$s_\xi = \left(\frac{.311}{|p - .311|}\right)^{2.08}. \tag{8}$$

It can also be shown, for $p < p_c$ and $s \gtrsim 5$, that every s-cluster has a boundary composed of

$$t_s = \left(\frac{1-p}{p}\right) s \tag{9}$$

$(-)$ vacuum sites.

Finally, we want to make one important remark. One can easily check using the formulae of this section that, on a given lattice, the number of s-clusters falls rather quickly with growing s. Hence there is an s_{max} such that the total number of s_{max}-clusters is 1. In other words, formation of clusters with s much larger than s_{max} is extremely improbable. This means that on a given lattice there exists an upper statistical cut-off on the size of observable clusters. This is, as discussed in section 7, a very important property of our scenario which allows us to avoid excessive microwave background distorsions due to large domain walls.

4. Biased Non-Equilibrium Phase Transitions in the Postinflationary Universe

We want to consider a universe that for some reason, perhaps due to the existence of an inflaton field, goes through a period of inflation and then settles down into the standard Friedman- Robertson-Walker (FRW) geometry. However, in addition, we postulate the existence of another scalar, ϕ, not the inflaton, which

has a potential with several degenerate (or almost degenerate) minima. As we said previously, in this paper we will assume that this potential is of the form (2). Furthermore, we will assume that

$$\frac{V_0}{\upsilon^2} << H_i^2 \tag{10}$$

and

$$V_0 << \upsilon^4 \tag{11}$$

where H_i is the Hubble constant during inflation. The first condition implies that during inflation, and long after, the potential force is much smaller than the cosmological friction, which justifies neglecting the potential until the universe is deep into the FRW expanding phase. The second condition guarantees that the ϕ field self couplings are weak. Since the only other interactions ϕ experiences are gravitational, this implies that ϕ is never in, or even near, thermal equilibrium. How small V_0 or how large υ is will be determined by our fit to the $\delta\rho/\rho$ data, and will be discussed below. As discussed above, we will call a field with these properties a "structuron", since the major role it plays in our scenario consists solely in inducing large scale structure formation. Detailed analysis of fluctuation-driven out of thermal equilibrium phase transitions in the post-inflationary universe will be presented in a separate paper [8]. Here we recall the main ingredients of this physics that we will need in the discussion below. We begin by stressing, once again, that the structuron is assumed to interact so weakly with itself and with other fields that it never comes close to thermal equilibrium. An out-of-equilibrium scalar field ϕ living on an inflating de Sitter space, observed over a physical volume ℓ^3, breaks into two pieces

$$\phi = \phi_c + \phi_q \tag{12}$$

where ϕ_c satisfies the classical equation of motion

$$\ddot{\phi}_c + 3H\dot{\phi}_c + \frac{\partial V}{\partial \phi_c} = 0 \tag{13}$$

(we have assumed that initial spatial gradient terms are exponentially driven to zero by inflation) with V the potential energy and H the Hubble parameter, and ϕ_q represents de Sitter space quantum fluctuations. During the inflationary de Sitter period $H = H_i$. However, equation (13) is also valid after inflation

has ended and the universe is in the FRW expanding phase. During inflation, and long afterward, H^2 is very large compared to the curvature of the potential. Hence, the $\frac{\partial V}{\partial \phi_c}$ term can be dropped to lowest order and $\phi_c = \vartheta$ where ϑ is an arbitrary constant. To next order, there is a tiny damped velocity $\dot{\phi}_c \sim \frac{V}{Hv}$. Hence, during inflation, and long afterward, ϕ_c is to very good accuracy an arbitrary constant. As already mentioned, ϕ_q represents quantum fluctuations of the scalar field in deSitter space. These fluctuations result in the formation of a weakly inhomogeneous quasi-classical random field. After inflation ends, the FRW horizon, $\ell_c = 1/H$, grows and fluctuations with scales less than the horizon are smoothed out. Thus ℓ_c acts as an UV cut-off in the momentum distribution of this random field. In a spatial region of length l, the distribution of the fluctuations around ϑ can be calculated and is given by

$$P(\phi) = \frac{1}{\sqrt{2\pi}\sigma_\ell} \exp\left(-\frac{(\phi - \vartheta)^2}{2\sigma_\ell^2}\right) \tag{14}$$

where

$$\sigma_\ell^2 = \frac{H_i^2}{4\pi^2} \ln\left(\frac{\ell}{\ell_c}\right) \tag{15}$$

Now, one can easily demonstrate [8],[9] that the longwavelength components in the Fourier decomposition of the random field ϕ_q are important. Therefore, the values of ϕ_q at any two distant points in the region of interest are, in general, not independent. This means the de Sitter space fluctuations introduce correlations among the values of the random field up to the maximal distance $H_i^{-1}e^n$, where n is the total number of e-folds during inflation. The above conclusions are strictly valid for a field which has been present in the universe since the beginning of the inflationary epoch. The situation with respect to long range correlations changes if the field ϕ is produced during inflation[1], let us say at x e-folds before the end of the inflationary period. Then, of course, the correlations in the random field are produced only up to the scale $\ell_x = H_i^{-1}e^x$, which may be much smaller than $H_i^{-1}e^n$. If the inflationary period prior to the appearence of the field ϕ is sufficently long, and provided that the microphysics producing ϕ fulfills certain, rather nonrestrictive, conditions [8], then the decomposition (12) remains valid.

[1]This may occur in a number of ways. For example, a complex scalar field with a large initial positive mass may, during inflation, undergo a phase transition (not to be confused with the structure transition) to a spontaneously broken theory with a massive radial field and a pseudo Goldstone boson ϕ.

In this case, however, correlations in the random field are restricted to scales smaller than ℓ_x. After inflation ends, the scale ℓ_x expands according to the expansion law of the subsequent FRW epoch, and at a given redshift $z \geq z_d$ equals approximately

$$\ell_x(z) = H_i^{-1}\, e^x \frac{T_r}{T_0} \frac{1}{(1+z_d)^{1/4}} (\frac{H_0}{H(z)})^{1/2} \tag{16}$$

where H_0, T_r, T_0, and z_d are the present Hubble constant, the temperature of reheating, the present microwave background temperature and the redshift at the beginning of matter dominance respectively. Hence the distribution describing the quasiclassical random field ϕ_q at some redshift z is that of (14) with arbitrary ϑ and σ_ℓ given by (15) for $\ell < \ell_x(z)$. Note that as long as $\sigma_{\ell_x} \leq \pi\upsilon$, that is

$$H_i \leq \frac{2\pi^2}{\sqrt{\ln(\ell_x/\ell_c)}}\upsilon \tag{17}$$

which we henceforth assume, then the distribution (14) will only be significant over the range of the two nearest neighbour vacua to $\phi_c = \vartheta$. Therefore, we need only consider physics near these two vacua, which we will call $(+)$ and $(-)$ respectively.

As long as H is much larger than $V_0^{1/2}/\upsilon$, the potential term in (13) can be ignored and the vacuum is well defined by the distribution (14) of fluctuations around an arbitrary constant ϑ. Eventually, long after inflation, $H(t)$ decreases so significantly that the potential term in the equation of motion becomes equal to, and then begins to dominate over, the damping term. We denote by z_t the redshift at which the potential term becomes non-ignorable. This is the redshift at which the phase transition is triggered. We will always assume that x is such that $\ell_c(z_t) < \ell_x(z_t)$.

We are now able to derive the percolation theory picture for domain wall formation. At z_t the field configuration ϕ within an horizon size volume, $\ell_c(z_t)^3$, is uniform due to the smoothing effects of the spatial derivative terms governing the evolution of the field. There are, however, fluctuations due to the components of the quasi-classical random field whose wavelengths λ satisfy $\ell_c(z_t) \leq \lambda \leq \ell_x(z_t)$. These fluctuations within a horizon volume are described by distribution (14) where σ_l given in (15) is to be evaluated at z_t. The field at z_t feels the potential and must decide into which of the two vacua it will roll under the potential force.

It is clear from Figure 1 that the probability that the system will roll into the (+) vacuum is

$$p = \int_{-\infty}^{0} P(\phi) d\phi \tag{18}$$

which, depending on the value of ϑ, can lie anywhere in the range $0 \leq p \leq 1$. Since ϑ is arbitrary, clearly p is arbitrary. It follows that the probability that the system will roll into vacuum $(-)$ is $q = 1 - p$.

After the phase transition is triggered, $\ell_x(z)$ grows according to the FRW expansion given in (16). The distance to the horizon, $\ell_c(z)$, also grows, but its rate of expansion is faster. Now, after z_t, the ϕ field rolls down the potential, oscillates and then settles in either the (+) vacuum or the $(-)$ vacuum. The redshift at which the system settles into one of these vacua is denoted by z_f, and can be considerably smaller than z_t. It is at z_f that truly topologically stable domain walls form. There are now two possibilities. The first is that $\frac{\ell_x(z_f)}{\ell_c(z_f)} \lesssim 1$. In this case, the causal horizon at z_f has "gobbled up" the region of ϕ correlations that had surrounded it at z_t. In this case, there are no correlations larger than the horizon at the time of domain wall formation and percolation theory can be employed. This is the case we will discuss in this paper. The second possibility is that $\frac{\ell_x(z_f)}{\ell_c(z_f)} >> 1$. In this case, domain walls with size larger than $\ell_x(z_f)$ still have a distribution given by percolation theory. However, at smaller scales there are non-zero correlations between causal horizons at the time of domain wall formation and, hence, percolation theory must be modified. We will discuss this second possibility in a later work.

We may conclude that, long after inflation has ended, the vacuum state of the system goes through a phase transition, choosing vacuum (+) with arbitrary probability p or vacuum $(-)$ with probability $q = 1 - p$. We emphasize that due to the nonequilibrium nature of this transition p can be arbitrary and need not, as in the case of thermal equilibrium, be equal to 0.5.

It is important to determine the value of the Hubble parameter at the redshift, z_t, at which the phase transition is triggered. The redshift at which the ϕ moves toward a definite vacuum is fixed by the condition that at that redshift the field should be able to change its value by the amount comparable to the distance

between the two minima within one Hubble time

$$\frac{1}{H(z_t)}\ |\dot{\phi}| \approx \pi\upsilon \tag{19}$$

Also, it is not hard to show that at z_t defined in this way all the terms in the equation of motion are comparable. This ensures that at z_t

$$3H(z_t)\dot{\phi} \approx -2\frac{\partial V}{\partial \phi} \tag{20}$$

where the factor of 2 on the right hand side takes care of the $\ddot{\phi}$ term. Combining these two results yields

$$H(z_t)^2 \approx \frac{2}{3\pi\upsilon}|\frac{\partial V}{\partial \phi}| \tag{21}$$

From what has been said about spatial correlations due to inflation, it follows that the fundamental length scale of the (+) and (−) vacuum domains, or the lattice spacing, is given by $H^{-1}(z_f)$. Let us define a parameter $\alpha \equiv H(z_t)/H(z_f) = \ell_c(z_f)/\ell_x(z_t)$. Also, since we prefer to refer to z_t, we will somewhat perversely denote $H^{-1}(z_f)$ by $\Lambda(z_t)$. It follows that

$$\Lambda(z_t) = \frac{\alpha}{H(z_t)} \tag{22}$$

where we will keep α as a free parameter in the forthcoming formulae. We will always refer to z_t, the difference between z_t and z_f being encoded in the factor α. If we take a specific value of α, then using formula (16) and assuming, for example, that $\ell_x(z_f) \approx \ell_c(z_f)$ one can estimate the time when the phase transition producing ϕ occured. It is not difficult to see that, with good reheating after inflation, $\alpha = O(10)$ requires $x = O(60)$.

Finally, we shall determine the size of our lattice. We are interested in the portion of the Universe at z_t which coincides with the present day visible horizon ($L(z = 0) = 6000h^{-1}$ Mpc). Hence we need only consider the finite lattice whose linear size is that of the present horizon scaled back to z_t

$$L(z_t) = L(0)/(1 + z_t) \tag{23}$$

The total number of lattice sites $N = (L(z_t)/\Lambda(z_t))^3$ is then easily found to be

$$N = (\frac{H(z_t)}{H_0}\frac{1}{\alpha(1 + z_t)})^3 \tag{24}$$

5. Energy Density Perturbations

Let us assume that the fundamental vacuum domains defined in the previous section form a cubic lattice. It follows from the discussion in the previous section that, at each lattice site, the system is in the (+) vacuum with arbitrary probability p where $0 \leq p \leq 1$, or in the (−) vacuum with probability $q = 1 - p$. Furthermore, the choice of vacuum state at any two different lattice points is uncorrelated. This situation defines a two-state percolation theory on our lattice. Moreover, we assume that at every link which separates two different vacua a domain wall forms with probability close to unity, as explained in [7]. Having at our disposal all the tools of percolation theory described in section 3, we are in a position to analyse the complete spectrum of density perturbations caused by these domain walls over a wide range of length scales.

In the following, we provide a detailed analysis for the strongly biased case where $p < p_c < q$. More specifically, we consider $0.1 < p < 0.2$, since results obtained in this regime have relatively simple structure and may be directly compared with experimental data as given in [4].

It has already been explained in [7] that the spatial structure of the percolation pattern in this interesting range of p is rather straightforward. There are compact bubbles of less favourable vacuum (+) surrounded by a sea of vacuum (−). Each bubble has a (fractalized) surface composed of a domain wall which stores a significant amount of energy. It is reasonable to assume that the walls assume their quasi- static shape sometime between z_t and z_f. From that point on, we can trace the evolution of domain wall "bags" and the energy deposited in those bags. Consider a bubble of s nearest neighbour (+) vacua, the s-cluster in terms of percolation theory. Its mean radius is well characterized by the average radius of gyration $R_s(p)$. Since, at z_t, the causal horizon is the lattice size, this radius is initially larger then the FRW horizon. However, the horizon radius grows at a faster rate than that of the bubble (whose radius just grows linearly with the expansion). Therefore, at some redshift $z_a(s)$, the bubble comes within horizon. From that point on the dynamics of the bubble becomes important. As indicated

by Widrow [10], a subhorizon-size bubble should first shrink under its surface tension, then undergo a few cycles of oscillations, finally radiating its energy in the form of scalar waves. Still, as the analysis of the spherical collapse model indicates, these bubbles are around sufficiently long to induce local inhomogeneities in the background medium. These inhomogeneities have the form of overdense regions composed of baryonic and dark matter gravitationally attracted to the bag wall. The energy that is stored in the domain wall surrounding an s-cluster at redshift z is easily computed from (5) and (9) to be

$$E_s = f t_s \sigma \Lambda(z)^2 \tag{25}$$

where f satisfies $1 \leq f \leq 6$. Since, in this paper, we are concerned with small p, we shall use a moderate value of $f = 3$. A discussion of the appropriate value of f would take us beyond the scope of this paper. Happily, the value of f does not substantially alter our quantitative or qualitative conclusions.

The spherical collapse model allows us to estimate the total mass accreted onto a seed of energy E_s by the time it disappears. The result is

$$M_s = \gamma_s E_s \tag{26}$$

where

$$\gamma_s = (\frac{4}{3\pi})^{2/3} (\frac{1+z_{app}}{1+z_{dis}})^{4/3} \tag{27}$$

and z_{app} and z_{dis} are the redshifts at which the seed appears and disappears respectively. Note that z_{app} and z_{dis} and, hence, γ_s can depend on s. Domain walls are fully formed at some redshift z_f. As discussed above, at this time all these walls are outside the FRW horizon, and matter does not substantially acrete to them. At redshift $z_a(s)$, however, the domain walls enter the horizon and the process of the effective matter acretion begins. Therefore, we will take $z_{app} = z_a(s)$. The detailed analysis of the evolution of the quasi-spherical domain wall in the FRW universe with a large cosmological damping term will be reported elsewhere [11]. In general, one expects that the presence of cosmological friction due to the expansion should slow down the oscillations with respect to those observed in flat space [10]. This gives a hint that the seed in the form of the domain wall bag may be around sufficiently long to cause the collapse of amounts of background matter significantly larger than the energy of the original seed.

Looking at the equation of motion for a scalar field one expects that γ_s becomes smaller for larger s, since larger s-clusters come within the horizon later, when the friction term becomes smaller. On the other hand, however, the larger s clusters have larger initial radii which makes the process of their "collapse" longer. Numerical investigation of the behaviour of thick and thin spherical domain walls in FRW background seems to confirm these expectations [11]. Hence, in this paper we simply assume the value of γ_s to be independent of s and of order 10, the order of magnitude supported by numerical analysis, although in specific cases one can get much larger values.

Putting all this together, some time after $z_a(s)$ but still at large redshifts, we are given local clumps of background matter corresponding to families of s-clusters. We can easily compute the mean energy density given by those clumps (we will continue to call them s-clusters although the original s-clusters are already gone). To this end we have to know the mean distance between s-clusters at the redshift of their formation. In what follows, we will take this redshift to be $z_a(s)$, the redshift when the original s-cluster enters the horizon, in accord with the discussion of the previous paragraph. Using percolation theory, we know the number of s-clusters on our lattice. It is given by $N_s = n_s(p)N$, where $n_s(p)$ and N are defined in (6) and (24) respectively. Hence the mean distance between s-clusters at redshift $z_a(s)$ in physical units is

$$d_s(z_a(s)) = \Lambda(z_a(s))\frac{1}{n_s(p)^{1/3}} = \frac{\alpha}{H(z_t)}\frac{1+z_t}{1+z_a(s)}\ \frac{1}{n_s(p)^{1/3}} \tag{28}$$

where $\Lambda(z_a(s))$ denotes the lattice spacing at $z_a(s)$. If we scale the above distance to the present time ($z = 0$), then we will get the present day observable scale over which the s-clusters contribute to the total energy density, $\lambda(s)$. Now, let us compute the energy density of s-clusters at $z_a(s)$. This is given by

$$\rho(s)|_{z_a(s)} = \gamma_s f\sigma\frac{1-p}{p}sn_s(p)\Lambda^{-1}(z_a(s)) \tag{29}$$

At this point, it is useful to compute $z_a(s)$ itself. It is easily obtained by equating the mean radius of gyration to the horizon at that redshift. We find that

$$1 + z_a(s) = \frac{1+z_t}{\alpha f_s(p)} \tag{30}$$

with

$$(1+z_t)^2 = \frac{H(z_t)}{H_0}(1+z_d)^{1/2} \tag{31}$$

where z_d is the redshift when the radiation dominated epoch ends and matter domination begins. The above formula holds for redshifts $z_a(s)$ larger that the redshift of the beginning of the matter dominance, but it will shortly be clear that that is the range of $z_a(s)$ of interest in this paper.

We are interested in our Universe, which is flat on the average, so we assume that the mean total energy density, which includes energy of all the components of the Universe, walls, dark matter, radiation, is equal to the critical energy density. One can easily express the critical energy density at $z_a(s)$ in terms of the present day critical density ρ_0

$$\rho_c(z_a(s)) = \rho_0 \frac{(1+z_a(s))^4}{1+z_d} \tag{32}$$

This formula is true only when $z_a(s) \geq z_d$, which we henceforth assume to be the case. Now we are ready to compute the energy density perturbation due to the s-clusters at $z_a(s)$. It is

$$\left.\frac{\delta\rho}{\rho}\right|_{z_a(s)}(s) = \gamma_s \frac{f\sigma H(z_t)}{\rho_0 \alpha} \frac{1-p}{p} s n_s(p) \frac{1+z_d}{(1+z_a(s))^3(1+z_t)} \tag{33}$$

From this point on, one should evolve the density perturbation computed at $z_a(s)$ to the present time using the full Einstein equations for adiabatic (metric) perturbation, see for example [12]. However, we can estimate the present energy density perturbation spectrum using well known results in the following approximate procedure. For small values of probability p the average distance between s-clusters at $z_a(s)$, which is the scale of the perturbation produced by those clusters, is larger than the horizon at $z_a(s)$. This average distance eventually comes within the FRW horizon at some smaller redshift which we call $z_h(s)$. There are two possibilities to be considered. The first is that $z_h(s)$ happens to be larger than or equal to z_d. In this case, $z_h(s)$ is easily computed to be

$$1 + z_h(s) = n_s(p)^{1/3}(1+z_t)/\alpha \tag{34}$$

and the perturbation grows between $z_a(s)$ and $z_h(s)$ by a factor of $\frac{(1+z_a(s))^2}{(1+z_h(s))^2}$, then between $z_h(s)$ and z_d by a logarithmic factor $1 + 2\log(\frac{1+z_h(s)}{1+z_d})$, and finally by the usual growth factor during the matter dominated epoch $1+z_d$. Putting everything together, one gets in this case

$$\left.\frac{\delta\rho}{\rho}\right|_{z=0}(s) = \gamma_s \frac{\alpha^2 f\sigma}{\rho_0} \frac{1-p}{p} s n_s(p)^{1/3} \frac{H_0^2}{H(z_t)} (1+z_d) f_s(p) (1 + 2\log\frac{1+z_h(s)}{1+z_d}) \tag{35}$$

(note that the reduced Hubble constant h does not appear explicitly either here or in (36)).

The other possibility is that $z_h(s)$ is smaller than z_d. In this case superhorizon growth of the perturbation in the radiation dominated epoch lasts till z_d and then is followed, as in the other case, by linear growth during matter dominance. It follows that

$$\left.\frac{\delta\rho}{\rho}\right|_{z=0}(s) = \gamma_s \frac{f\sigma}{\rho_0}\frac{1-p}{p} s n_s(p) H_0 f_s(p) \frac{1}{(1+z_d)^{1/2}} \tag{36}$$

As discussed above, the s which enters the formulae for overdensities has to be expressed in terms of the corresponding physical scale $\lambda(s)$. We find that

$$\lambda(s) = (1+z_a(s))\Lambda(z_a(s))\frac{1}{n_s(p)^{1/3}} = \frac{\alpha}{H(z_t)}(1+z_t)\,\frac{1}{n_s(p)^{1/3}} \tag{37}$$

The formulae (35) and (36) together with (37) constitute the main result of this section. They give the continuous spectrum of energy density fluctuations due to the formation of domain walls during the biased phase transition of the structuron field. These fluctuations should be added to those produced by the inflaton itself in order to obtain the total spectrum of fluctuations which may be compared with observations. Numerical analysis of the spectrum and comparison with QDOT [4] results are presented in the next section. For the sake of completeness one should notice here that the range of λ, or equivalently s, over which the analytical results (35) and (36) are valid is in fact restricted for two reasons. Firstly, because the validity of the expression for $n_s(p)$ which we are using here has been established in reference [7] only over a finite, although wide, range of s. Secondly, because the formula for $R_s(p)$ changes for $s < s_\xi$ taking the form relevant for the critical region. These limitations and assumptions about the range of z's considered are checked a'posteriori for numerical examples discussed in the following sections.

6. Fits of wall-induced density fluctuations to experimental data

The extensive IRAS survey has allowed construction of detailed maps and quantitative analysis of the large scale structure of the Universe out to roughly 140 h^{-1}Mpc. Using this data one can construct the density field of galaxies and,

by adding some theoretical assumptions, one can infer the mass density distribution and the pattern of peculiar velocities in the Universe [2]. These experimental results can serve as a gauge for theoretical models of large scale structure formation. In particular, one can test the pure cold dark matter model, [3], perhaps the most popular model over the last decade, and very well motivated by fundamental particle theory. In this paper we will use the analysis presented in [4] based on the QDOT redshift survey [2]. This analysis shows that CDM with primeval fluctuations of Harrison-Zeldovich type, generated for example during an inflationary period in the early Universe, cannot alone account for the whole spectrum of energy density perturbations. If one normalizes the CDM spectrum in such a way that it accurately fits the observed spectrum at small scales, up to 5 h^{-1}Mpc, then there is a statistically significant disagreement at larger scales, where it is found that the CDM prediction falls well below the observed spectrum. The plot in Figure 2 presents the difference between CDM simulations and observational data, as reported by Saunders et al. [4] (the uncertainties associated with measurements at larger scales are shown as two vertical lines). The particular CDM spectrum which has been used is normalized in such a way that $b_I\sigma_8 = 0.69$ as found for IRAS galaxies in [4]. Here the b_I is the linear bias factor (I stands for IRAS) and σ_8 is the rms matter density fluctuation in spheres of radius 8 h^{-1} Mpc, the quantities usually used for normalizing theories of large scale structure. In this paper we choose to work with the inflationary CDM spectrum normalized so that it accurately describes small scale data instead of normalizing it, for instance, at the COBE point. We feel more comfortable with this normalization, as the amount of data available in the range of smaller scales is extensive with its structure carefully studied, and also because the physical length scales parametrizing the potentials discussed in this work correspond to these smaller cosmological scales.

The main numerical result of this paper is shown in Figure 3. The curves (a),(b),(c) represent our fits of the domain wall-induced overdensity spectrum (35), (36) in models with a potential in the form (2), to the difference between pure CDM (with Harrison- Zeldovich primeval fluctuations) and the observed rms energy density spectra, as given by QDOT [2], [4], on scales between 20 Mpc h^{-1} and 80 Mpc h^{-1} (for the simplicity of presentation we put the reduced

Hubble constant h=1 from this point on)[2]. The plots (a), (b) and (c) in Figure 3 correspond to $p = 0.11$, 0.13, and 0.15 respectively. They are all calculated using $\alpha = 10$ and $\gamma_s = 10$, realistic values for these parameters as verified by direct computations. A selection of numerical values of $\frac{\delta\rho}{\rho}$ for the three different curves in Figure 3 and the corresponding values for the curve in Figure 2 are shown in Table 1. The sets of parameters of the potential corresponding to the different curves in Figure 3 are given in Table 2. All the plots are normalized in such a way that their peaks correspond to the scale of 30 Mpc (which fixes the mass parameter m for given p) and that their maximal height is 0.187 (which in turn fixes the height of the potential or the symmetry breaking scale v for fixed p, m and α). One can see that the fits give very tiny masses in all the cases and symmetry breaking scales v of about 6×10^{13} GeV. It follows from (17) that the associated values of H_i are of the order 10^{14} GeV, near the present upper limits on the inflationary Hubble constant. It is interesting to note that these values of parameters may arise in a wide range of well motivated particle models. Even such tiny masses as the ones discussed here may be stable against radiative corrections if protected by exact or nearly exact symmetries as happens in the models of ref [6],[5].

Analyzing the plots (a), (b), (c) in Figure 3 one can see that the smaller the probability p is the larger the slope of the curve at small and large scales. The character of the curves may be understood by noting that they represent the superposition of two effects acting in opposite directions. One is the number of s-clusters which is large at small scales (hence, small s) and falls down quasi-exponentially toward large scales. The other is the amount of energy stored in the boundary of an s-cluster which is proportional to s, hence small at small scales and rising toward large ones. Table 2 contains the values of s which correspond to the lower and upper limiting scales considered in this paper. First of all, one can see that the s giving rise to perturbations at the lower end of the domain of

[2]It has already been noted that the reduced Hubble constant h drops out from the formulae (35), (36). In fact it is present there only implicitly through the value of z_d. On the other hand, it may be seen from (37) that since $H(t)$ is determined up to a factor h, the physical scale corresponding to a given s is multiplied by h^{-1}, the same factors which enters all measured distances. Hence, with changing h, all our fits and the data curve from Figure 2 are to a good approximation simply scaled horizontally by a common factor.

our plots, s(20 Mpc), are in all the cases larger than the respective percolation correlation length s_ξ. In fact, it is possible to continue the percolation spectra down below s_ξ, but this requires some further analysis at the level of percolation theory, which is beyond the scope of this work. For this reason we do not attempt here to compare our results to QDOT data for scales below 20 Mpc. Next, one can easily check that the values of s corresponding to the upper edge of the scale interval we consider here, see the s_{COBE} column in Table 2, fall within the domain of applicability of the percolation formulae listed in Section 3.

All the curves in Figure 3 are normalized to fit the difference between QDOT data and CDM predictions on scales smaller than 80 Mpc. It is clear that density fluctuations induced by structure transitions accurately account for this difference, both in magnitude and in the shape of the distribution. We point out that this distribution is a natural consequence of three-dimensional percolation theory, its shape being set by the basic laws governing percolation.

An important independent check for our statistical picture of large scale structure formation is the computation of density perturbation at the COBE scale (for h=1 it is 730 Mpc) and comparison of these numbers with the result reported by Smoot et al. [1], $\frac{\delta T}{T}|_{COBE} = 1.1 \times 10^{-5}$. The volume s_{COBE} of clusters responsible for fluctuations at the scale of 730 Mpc is found easily by inverting the formula (28) and using (21), (30), and (31). If one computes $z_a(s_{COBE})$, then it turns out that this redshift happens to be much larger than z_d. This means that clusters producing fluctuations at the COBE scale disappear long before the matter dominance epoch. It follows that gravitational potential fluctuations which give the dominant contribution to the microwave background anisotropy at large scales come from fluctuations induced by walls in the surrounding matter, both dark and baryonic, and not from actual domain walls entering the horizon at the time of decoupling or later. It may easily be demonstrated that the direct contribution to fluctuations given by walls whose radii become smaller than the FRW horizon at small redshifts is subdominant by computing the number of such walls expected within the visible horizon. This is done using formula (30), assuming $z_a(s)$ to be of the order of z_d or smaller and then using (6) and (24). The numbers corresponding to $z_a = z_d$ are given in Table 3 in the columns labelled s_a, the volume of the cluster whose radius of gyration enters horizon at z_d, and N_{s_a},

the total number of such clusters expected. It is clear that the contribution to the microwave background anisotropy at large scales coming from large bubbles is very strongly statistically suppressed (for further discussion of this point see section 7) and subdominant with respect to the effect resulting from wall-induced fluctuations in dark and baryonic matter.

As may be seen from Table 2, all our cases can easily account for the COBE measurements, predicting fluctuations of $\delta T/T$ exactly of the required order of magnitude (we use the standard Sachs-Wolfe formula to convert $\delta\rho/\rho$ into $\delta T/T$)[3]. In addition to the magnitude of the $\delta T/T$ anisotropy, the COBE experiment [1] also gives the value of the fluctuation spectral index n=1.15 $\pm$ 0.6 . Index n is defined through the power-law ansatz for the power spectrum of primordial fluctuations $P(k) = |\delta_k|^2 = Ak^n$, where δ_k is the Fourier transform of the over-density field $\delta\rho/\rho$. However, as analyzed in detail by Scaramella and Vittorio [16], to judge the viability of models predicting specific values of n one has to take carefully into account the effect of cosmic variance. The reason for this is that different cosmic observers look at different skies which, in turn, are different realizations of the density field. One has to ask the question of how many observers would see a realization of the sky consistent with data for a value of n predicted by a given model. It is shown in reference [16] that more than 50% of the observers could see a sky which gives a good fit to the COBE data as long as $-1.5 < n < 2.5$. In the present case, given the analytical formula (36), we can easily compute the best values of n for different percolation probabilities p. The values which give the best fits of the power law ansatz for the power spectrum to our model between the COBE scale, 730 Mpc, and 2000 Mpc are listed in the last column of the Table 2. Obviously, all the cases we consider lie well within the limits given by Scaramella and Vittorio. We note that the larger the probability p the closer is the predicted spectral index n to the value n=1.15.

[3]Of course, as discussed for instance in [13], [14], given a model of inflation one can try to explain the COBE measurement by gravitational waves produced during inflation, but the magnitude of this effect is strongly model dependent. Since we do not rely in our analysis on any specific model of inflation, there is no inconsistency in obtaining, at the COBE scale, domain wall contributions comparable to the COBE result. We can always restrict ourselves to models with a low power polynomial potential, like chaotic inflation, where the gravitational waves contribution can be shown to be subdominant [14].

It should be stressed that our results are obtained without any extreme fine-tuning. Curves corresponding to p between 0.11 and 0.15 are very close to each other and similar stability of the results holds with respect to small changes in all remaining parameters. For example, in all the above cases we have taken $\gamma_s = 10$. One should note, however, that even taking $\gamma_s = 1$ gives reasonable model parameters and it is clear that taking $\gamma_s > 10$ would produce acceptable examples of models with smaller values of the symmetry breaking scale υ required to fit the magnitude of the experimental spectrum.

7. Microwave background distorsions

The walls that disappear by z_d (well before decoupling of photons) do not cause any direct perturbation to the microwave background. They induce energy density perturbations in background matter (dark and baryonic) and those perturbations are standard effects, believed to be innocuous if the resulting amplitude of theoretical fluctuations agrees with the observed one (it is our attitude to normalize our spectra in exactly this way). There are, however, additional effects due to walls which annihilate late, during the epoch of recombination and after. Radii of these bubbles are of the order of the horizon scale at decoupling and larger (≥ 100 Mpc at present), and, as discussed in [15], such bubbles collapsing after decoupling form a time dependent gravitational potential which produces a shift in the frequencies of the photons passing through them. The estimate of corresponding distorsions to the $\delta T/T$ of the photon background, assuming that walls are actually present within our horizon, is [15]

$$\frac{\delta T}{T} \approx 8\pi G\sigma H_0^{-1} \tag{38}$$

Demanding that $\delta T/T \leq 5 \times 10^{-5}$ (the limits on $\delta T/T$ at small angular scales $\theta < 1^o$ are less restrictive than at large scales) and naively using (38) one gets

$$\sigma \leq 5 \times 10^{-9}\mathrm{GeV}^3 \tag{39}$$

which is rather restrictive (see Table 3) and at first sight cannot be satisfied in the examples discussed here. However, our calculation tells us that the probability of seeing such a large bag of wall is extremely tiny. In fact, the actual $\delta T/T$ due to these walls should be weighted by the square root of the average number

of a given size wall-bags on our lattice, $\sqrt{N_s}$, assuming that photons perform a random walk among wall-bags. This weighting number is always smaller than $\sqrt{N_{s_a}}$, where s_a is the volume of the cluster which enters the horizon at ${z_d}^4$. If we weight in this way the right hand side of (38), we then get numbers respecting the above quoted upper limit on $\delta T/T$ with a wide margin in all of our examples, as may easily be seen from Table 3.

8. Conclusions

In this paper we have described the contribution to cosmological energy density fluctuations coming from topological defects in the form of domain walls produced during a biased phase transition in the vacuum of a light, weakly interacting scalar field, which we call the structuron. We have used as an example a transition triggered by inflationary quantum fluctuations, but the shape of spatial statistics of the defects, and consequently the spectrum of their contribution to the overall energy density fluctuations, will be similar for any other biased phase transition. Using percolation theory methods we have been able to describe in an analytical way the average properties of the spatial pattern formed by walls after a transition of this type. Applying the results to a simple cosine potential, naturally arising in particle models with light scalars, we are able to produce an additional contribution to the mean cosmological energy density which has sufficient power at larger scales to account for the apparent difference between the cold dark matter spectrum normalized at small scales and the total IRAS spectrum. As a bonus, after continuation of our spectra beyond the range of small and intermediate scales, which they successfully describe, up to the COBE scale, we find at that scale a contribution which is precisely of the order of the COBE result. Thus, structure transitions offer a nontrivial way of understanding nonzero microwave background distorsions at very large cosmological scales. Also note that the nonequilibrium phase transitions which we discuss, the structure transitions, naturally occur well before decoupling, deep in the radiation domi-

[4]In this paper z_d denotes the beginning of matter dominance. However, since the last scattering surface has a significant thickness, and since its redshift is not that much smaller than z_d, we compute all the limits here using z_d, which is a rather conservative procedure in the present case.

nated epoch, and, therefore, can evade problems that arise in models with truly late time phase transitions.

It is worth of pointing out that using phase transitions which allow a percolative description of the resulting vacuum structure for generating large scale cosmological structure is a nontrivial and novel approach. In standard scenarios to explain physical phenomena at a given scale, one needs some causal physics operating at that scale, or in other words, significant correlations extending over that scale. In our approach we exclusively use small scale correlations operating over a fundamental domain whose size is orders of magnitude smaller than the distance to the FRW horizon. The whole large scale pattern arises as a random, stochastic superposition of independent small scale choices. It is the astonishing property of such a statistical system that it displays regular features, described by percolation theory, which closely correspond to regularities observed in the distribution of matter in the Universe.

Acknowledgements

Z. Lalak was supported by The Royal Society and by Alexander von Humboldt Foundation. S. Lola was supported by the Greek State Scholarships Foundation.

References

[1] G.F.Smoot et al., Astrophys. J. Lett. 396, L1 (1992).

[2] M.Rowan-Robinson et al., Mon.Not.R.astr.Soc. 247, 1 (1990); G.Efstathiou et al., Mon.Not.R.astr.Soc. 247, 10p (1990); W.Saunders et al., Nature 349, 32 (1991); N.Kaiser et al., Mon.Not.R.astr.Soc. 252, 1 (1991); M.Rowan-Robinson et al., Mon.Not.R.astr.Soc. 253, 485 (1991); W.Saunders,M.Rowan-Robinson,A.Lawrence, Mon.Not.R.astr.Soc. 258, 134 (1992).

[3] M.Davis,F.J.Summers,D.Schlegel, Nature 359, 393 (1992); A.N.Taylor, M.Rowan-Robinson, Nature 359, 396 (1992); W.Saunders, M.Rowan-Robinson,A.Lawrence, Mon.Not.R.astr.Soc. 258, 134 (1992).

[4] W.Saunders,M.Rowan-Robinson,A.Lawrence, Mon.Not.R.astr.Soc. 258, 134 (1992).

[5] S.Lola, G.G.Ross, Nucl.Phys. B406, 452 (1993).

[6] C.T.Hill,G.G.Ross, Nucl.Phys. B311, 253 (1988),Phys.Lett. B203, 125 (1988); B.Ovrut,S.Thomas, Phys.Lett. B277, 53 (1992); A.Gupta,C.T.Hill, R.Holman, E.Kolb, report FNAL-PUB91/167 (1991).

[7] Z.Lalak, B.Ovrut, S.Thomas, report CERN-TH.6957/03, UPR-0507T.

[8] Z.Lalak, S.Lola, B.Ovrut, G.G.Ross, manuscript in preparation.

[9] For an introduction to inflationary cosmology see: A.Linde, *Particle Physics and Inflationary Cosmology*, Harwood Academic Publishers, 1990.

[10] L.M.Widrow, Phys.Rev. D40, 1002 (1989).

[11] Z.Lalak,S.Lola,B.Ovrut,G.G.Ross, work in progress.

[12] E.Kolb,M.Turner, *The Early Universe*, Addison-Wesley Publishing Company, 1990, and references therein.

[13] L.Krauss,M.White, Phys.Rev.Lett. 69, 869 (1992).

[14] R.L.Davis,H.M.Hodges,G.F.Smoot,P.J.Steinhardt,M.S.Turner, Phys.Rev. Lett. 69, 1856 (1992).

[15] A.Stebbins,M.S.Turner, Astrophys.J.Lett. 339, L13 (1989); M.S.Turner,R.Watkins,L.M.Widrow, Astrphys.J.Lett. 367, L43 (1991); G.Goetz,D.Notzold, Nucl.Phys. B351, 645 (1991).

[16] R.Scaramella,N.Victorio, Mon.Not.R.Astron.Soc. 263, L17, (1993).

X h^{-1}Mpc		Y		
	Δ	p=0.11	p=0.13	p=0.15
20	0.18	0.178	0.181	0.173
30	0.181	0.187	0.187	0.187
40	0.174	0.170	0.169	0.174
50	0.149	0.142	0.136	0.149
63	0.117	0.103	0.1	0.109
80	0.09	0.067	0.07	0.073

Table 1

p	m GeV	υ GeV	s_ξ	$s(20\ Mpc)$	s_{COBE}	$\frac{\delta T}{T}\|_{COBE}$	n
0.11	3×10^{-32}	6.3×10^{13}	2.48	3.3	39.6	1.4×10^{-5}	2.20
0.13	5×10^{-32}	6.3×10^{13}	3.08	4.5	50.5	1.3×10^{-5}	2.12
0.15	4.5×10^{-32}	7.1×10^{13}	3.93	4.36	59.8	1.7×10^{-5}	2.06

Table 2

p	s_a	N_{s_a}	σ GeV^3
0.11	843	8×10^{-65}	2.4×10^{-4}
0.13	1385	2×10^{-66}	0.4×10^{-3}
0.15	1385	5×10^{-66}	0.45×10^{-3}

Table 3

Figure Captions

Figure 1. The probability distribution P of the random field ϕ_q around an arbitrary mean value ϑ superimposed on top of the cosine potential V. The horizontal axis gives values of ϕ/ϑ, the units on the vertical axes are arbitrary. Two minima of the potential are shown, the left minimum corresponds to the (+) vacuum, the right one to the (–) vacuum.

Figure 2. The difference between energy density overdensities, $\frac{\delta\rho}{\rho}\Big|_{QDOT} - \frac{\delta\rho}{\rho}\Big|_{CDM}$, given by the QDOT analysis of the IRAS data and generated in the CDM scenario with a Harrison-Zeldovich spectrum of primeval fluctuations [4]. Axis X represents physical scales in Mpc h^{-1}, axis Y gives values of the difference between overdensities. The two vertical lines represent uncertainties of measurements at larger scales.

Figure 3. Wall-induced energy overdensity spectra in models defined in Tables 2 and 3. Curves (a), (b), (c) correspond to p=0.11, 0.13, 0.15 respectively. Axis X represents physical scales in Mpc h^{-1}, axis Y gives values of overdensities.

Figure 4. Superposition of plots from Figures 2 and 3. The dashed curve (d) is the QDOT data curve from Figure 3.

Table Captions

Table 1. Numerical values of overdensities depicted in the Figures 2 and 3. The column labelled Δ corresponds to the curve from the Figure 2 and contains data taken from [4].

Table 2. Parameters of the models generating spectra from the Figure 3. The last two columns give predictions for the magnitude of the microwave background anisotropy at the COBE scale and for the spectral index of fluctuations at large scales.

Table 3. This table illustrates statistical suppression of population of large bubbles in the percolation theory picture. The last column gives values of the wall tension in models discussed in the paper.

Figure 1

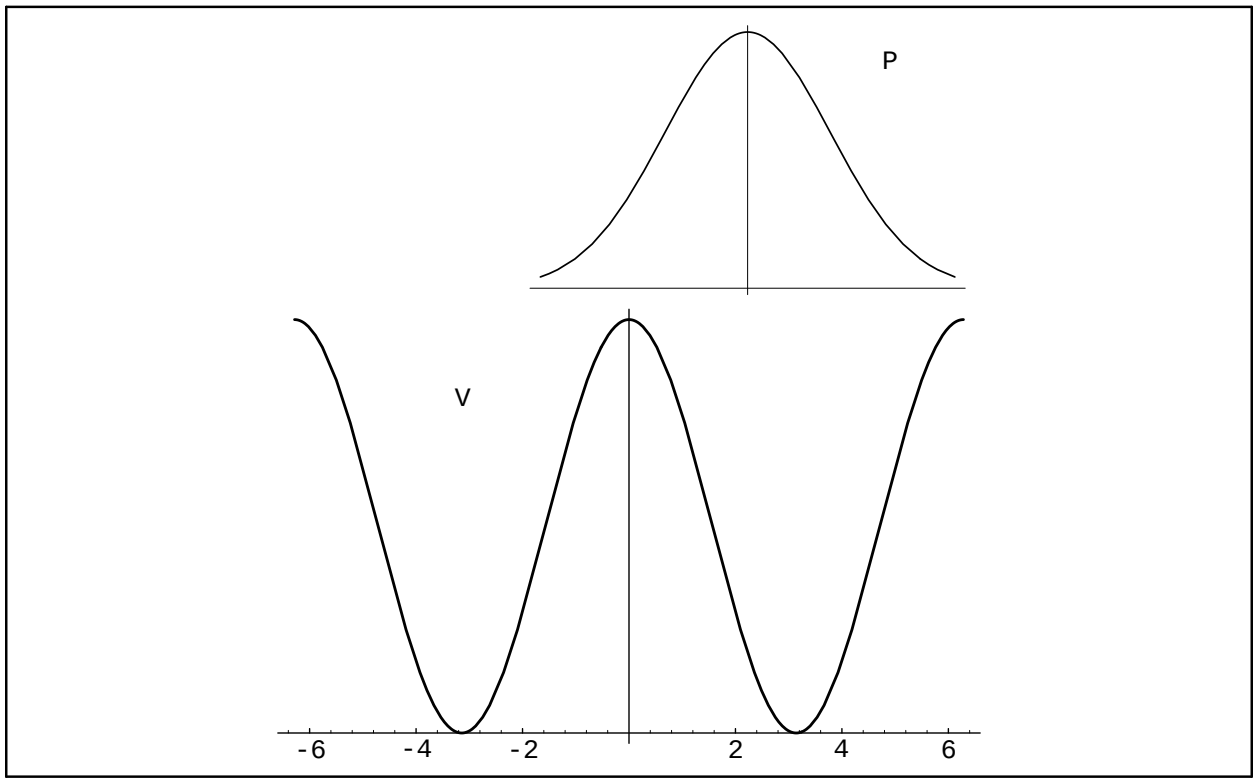

This figure "fig1-1.png" is available in "png" format from:

http://arXiv.org/ps/hep-ph/9404218v3

This figure "fig1-2.png" is available in "png" format from:

http://arXiv.org/ps/hep-ph/9404218v3

Figure 2

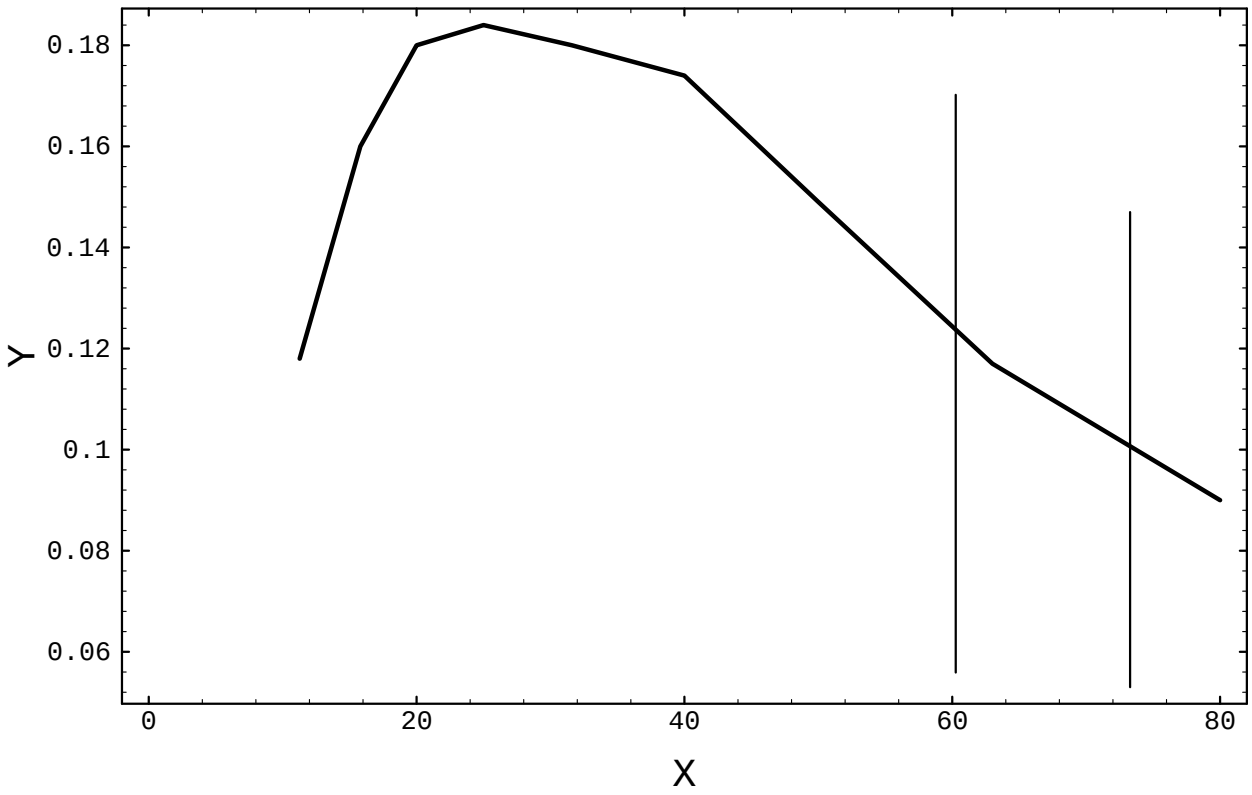

This figure "fig1-3.png" is available in "png" format from:

http://arXiv.org/ps/hep-ph/9404218v3

Figure 3

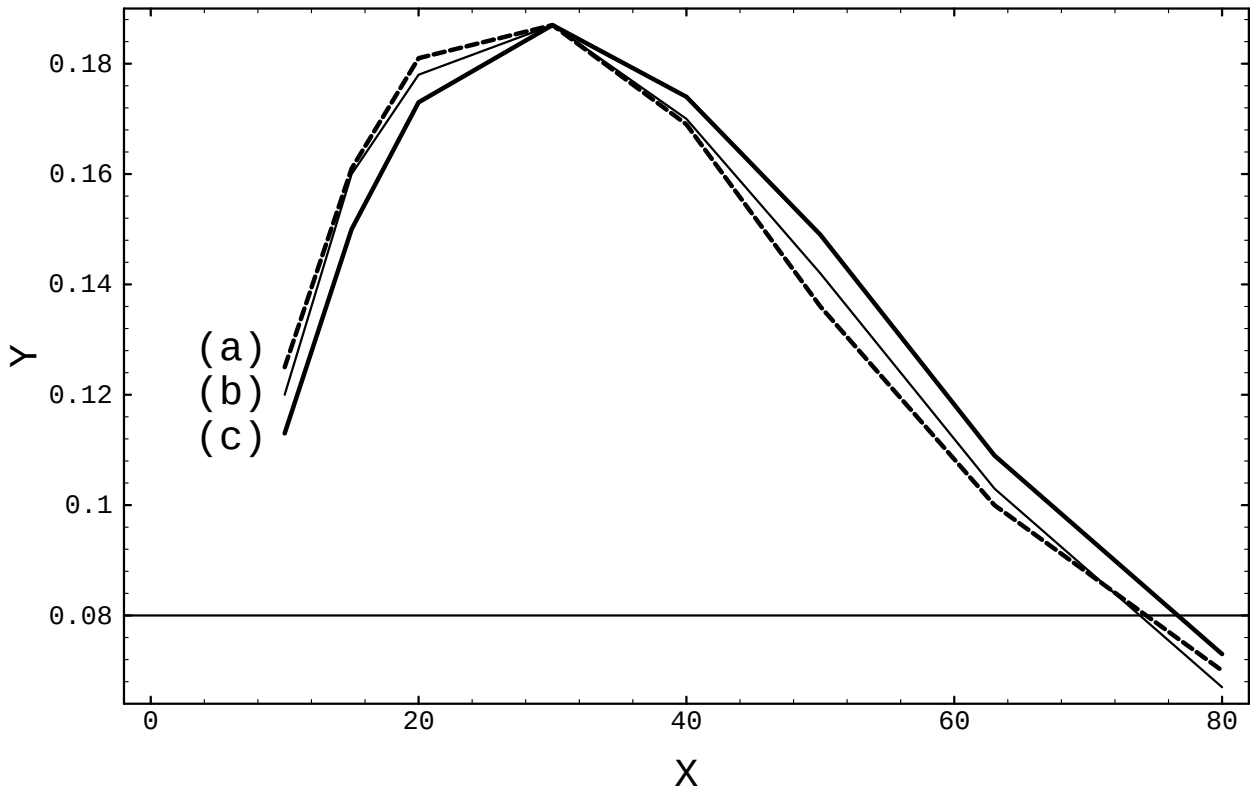

This figure "fig1-4.png" is available in "png" format from:

http://arXiv.org/ps/hep-ph/9404218v3

Figure 4